Submitted to ApJL. Draft version dated April 21, 2016.
Preprint typeset using LaTeX style emulateapj v. 12/16/11

FRONTIER FIELDS CLUSTERS: THERMODYNAMICS OF THE LARGE-SCALE FILAMENT CROSSING MACS J0717.5+3745

G. A. Ogrean[1, †], C. Jones[2], T. Whalen[3], R. J. van Weeren[2, ‡], W. Forman[2]

[1]KIPAC, Stanford University, 452 Lomita Mall, Stanford, CA 94305, USA; gogrean@stanford.edu
[2]Harvard-Smithsonian Center for Astrophysics, 60 Garden Street, Cambridge, MA 02138, USA; and
[3]University of Maryland, College Park, MD 20742, USA;
Submitted to ApJL. Draft version dated April 21, 2016.

ABSTRACT

We present results from deep *Chandra* observations of the large-scale filament extending SE from the Frontier Fields cluster MACS J0717.5+3745. The gas within the filament is found to have a temperature of $1.58^{+0.51}_{-0.25}$ keV and a density of $\sim 10^{-4}$ cm^{-3}. The filament density corresponds to a high baryon over-density of ~ 250, which can be explained by the fact that we are probing only the densest part of the filament. The filament properties are consistent with numerical simulations and with the few other observational results reported to date. Within the filament, ~ 2 Mpc away from the cluster center, there is a galaxy group with a mass of $\sim 5 \times 10^{13}$ M$_\odot$ and a temperature of ~ 3 keV. This group is likely infalling for the first time towards the cluster. NW of the cluster, ~ 670 kpc from the center, there is a ram pressure-stripped core that appears to have traversed the densest parts of the cluster after entering the ICM from the direction of the filament. This core is probably a later stage of the galaxy group seen in the filament. We detect a density discontinuity N-NE of the core, which we speculate is associated with a cold front. We do not detect a temperature jump across the density discontinuity. The non-detection is likely caused by a combination of poor count statistics and multiple superimposed substructures.

Keywords: Galaxies: clusters: individual: MACS J0717.5+3745 — Galaxies: clusters: intracluster medium — X-rays: galaxies: clusters

1. INTRODUCTION

In the ΛCDM cosmological model, structure in the Universe is organized in a filamentary web in which large-scale cosmic filaments connect virialized massive structures such as clusters and groups of galaxies (e.g., Einasto et al. 1994). Approximately a third of the total bayonic matter is expected from hydrodynamic simulations to be contained in these large-scale filaments (e.g. Davé et al. 2001), in the form of low-density gas with temperatures of $10^5 - 10^7$ K. One of the main signatures of cosmic filaments is soft X-ray emission. However, the low density of the gas within the filaments poses a significant observational challenge, which causes detections to strongly depend on fortuitous alignments of the filaments with our line of sight. As a consequence, there have been only a handful of filament detections, among which the one in MACS J0717.5+3745 (Ebeling et al. 2004), the one between A222-A223 (Dietrich et al. 2005; Werner et al. 2008), and several in A2744 (Eckert et al. 2015).

Clusters of galaxies grow via the infall of gas and less massive structures along cosmic filaments (e.g., Springel et al. 2006). During infall and subsequent collision with the cluster, less massive structures will be ram-pressure stripped as they fly through the cluster's denser regions. Consequently, depending on their original density, these structures are either fully destroyed, or their compact cores survive and develop tails in their wake. An example of the latter scenario is seen in the cluster 1E 0657–558 (Elvis et al. 1992), in which the collision of a massive cluster with a cluster about 1/10 of its mass (Springel & Farrar 2007; Mastropietro & Burkert 2008) resulted in the famous "bullet" morphology of the less massive structure (Markevitch et al. 2002).

Here, we present results from *Chandra* observations of the merging galaxy cluster MACS J0717.5+3745. MACS J0717.5+3745 ($z = 0.546$; Ebeling et al. 2001, 2007) is one of the most complex merging systems discovered to date, being the site of collisions between four substructures (Ma et al. 2009; Medezinski et al. 2013). The superposition of the dark matter halos of these substructures also makes MACS J0717.5+3745 the largest known gravitational lens (Zitrin et al. 2009; Medezinski et al. 2013). The analysis of shallower *Chandra* observations of the cluster by Ma et al. (2009) found hot regions with temperatures ~ 20 keV, remnant cool cores with temperatures of ~ 5 keV, and density and temperature jumps at the interface between the cluster and the SE filament. The authors speculated that the jumps are caused accretion of gas from the filament onto the cluster. More recently, we have analyzed the thermodynamical properties of the ICM of MACS J0717.5+3745 using deeper *Chandra* observations (van Weeren et al., submitted). In this letter, we present the physical properties of the SE filament connected to MACS J0717.5+3745, and those of the substructures along the filament.

In Section 2, we summarize the processing of the *Chandra* datasets. The properties of the filament are discussed in Section 3, while those of the substructures in the filament are discussed in Section 4. The properties of the

† Hubble Fellow
‡ Clay Fellow

NW core that flew through the cluster are presented in Section 5. Our conclusions are summarized in Section 6.

Throughout the paper we assume a ΛCDM cosmology with $H_0 = 70$ km s^{-1} Mpc^{-1}, $\Omega_m = 0.3$, and $\Omega_\Lambda = 0.7$. For these parameters, 1 arcmin at the redshift of MACS J0717.5+3745 ($z = 0.546$) corresponds to a linear distance of approximately 383 kpc.

2. DATA PROCESSING AND BACKGROUND MODELING

Chandra observed MACS J0717.5+3745 four times between Jan 2001 and Dec 2013, for a total of 243 ks. Of the four ObsIDs, two (1655 and 16235) were taken in FAINT mode, while the other two (4200 and 16305) were taken in VFAINT mode. More details about the observation parameters can be found at the Chandra Data Archive.

The ObsIDs were reprocessed to apply the newest calibration files as of Jan 2004. Time periods affected by soft protons were removed from the data using the CIAO script *deflare*. ObsID 1655 had residual soft proton flares and we decided to remove it from the spectral analysis. The total clean exposure time after flare filtering was approximately 209 ks (193 ks ignoring ObsID 1655). Point sources were detected in the energy bands $0.5 - 2$ and $2 - 7$ keV using the script *wavdetect*, were visually confirmed, and excluded from the analysis. The instrumental background was subtracted using the stowed background files available in CalDB 4.6.3. Before subtraction, the instrumental background files were normalized to have the same $10 - 12$ keV count rate as the corresponding source files.

The sky background was modeled as the sum of unabsorbed emission from the Local Hot Bubble, absorbed emission from the Galactic Halo, and absorbed emission from unresolved X-ray sources. The hydrogen column density was fixed to 8.36×10^{20} cm^{-2}, corresponding to the sum of the atomic and molecular hydrogen column densities in the direction of MACS J0717.5+3745[4] (Kalberla et al. 2005; Willingale et al. 2013). All the foreground components were assumed to have solar metallicities equal to those reported by Feldman (1992).

A more detailed description of the data processing and the background modeling is provided by van Weeren et al., submitted. Our analysis can also be reproduced by the reader by downloading the datasets from the Chandra Data Archive and running the JUPYTER notebook[5] available at https://github.com/gogrean.

3. LARGE-SCALE COSMIC FILAMENT

To define the region of the filament that is least contaminated by ICM emission, we examined the surface brightness profile in a rectangular region aligned with the filament. In this region, the surface brightness decreases away from the cluster center, and then increases again when the region intersects the SE group located along the filament; there is no radial range in this region where the surface brightness is flat. This suggests that the ICM of MACS J0717.5+3745 contaminates the filament, and this contamination needs to be considered when modeling the filament emission.

To model the filament and the contamination from the ICM, we extracted spectra in three rectangular regions:

[4] http://www.swift.ac.uk/analysis/nhtot/index.php
[5] Running the notebook requires the bash_kernel package.

Table 1
Parameters of the regions used for the spectral analysis. The regions are shown in Figure 1. Uncertainties are quoted at the $\Delta C = 1$ level.

FOREGROUND AND BACKGROUND

Model Component	Temperature[a]	Normalization[b]
Local Hot Bubble	$0.135^{+0.007}_{-0.008}$	$7.21^{+0.30}_{-0.18} \times 10^{-7}$
Galactic Halo	$0.59^{+0.09}_{-0.08}$	$2.78^{+0.45}_{-0.44} \times 10^{-7}$
Unresolved Background Sources ObsID 16235/16305	–	$4.44^{+0.35}_{-0.37} \times 10^{-7}$
Unresolved Background Sources ObsID 4200	–	$7.02^{+0.49}_{-0.58} \times 10^{-7}$

LARGE-SCALE FILAMENT

Model Component	Temperature[a]	Normalization[b]
On Filament	$1.58^{+0.51}_{-0.25}$	$4.00^{+0.56}_{-0.60} \times 10^{-5}$
Off Filament	$11.55^{+9.09}_{-3.95}$	$1.55^{+0.14}_{-0.10} \times 10^{-5}$

GROUP IN THE FILAMENT

	Temperature[a]	Normalization[b]
	$3.87^{+0.66}_{-0.51}$	$(1.77 \pm 0.13) \times 10^{-4}$

FLY-THROUGH CORE

Model Component	Temperature[a]	Normalization[b]
Core	$6.82^{+1.88}_{-1.36}$	$3.41^{+0.29}_{-0.25} \times 10^{-4}$
N+S of Core	$7.47^{+1.11}_{-0.86}$	$2.08^{+0.77}_{-0.78} \times 10^{-4}$
Ahead of Core	$5.06^{+1.61}_{-0.98}$	$8.52^{+0.88}_{-0.77} \times 10^{-5}$
Behind Core	$10.89^{+2.05}_{-1.27}$	$3.92^{+0.10}_{-0.09} \times 10^{-4}$

[a] Units of keV.
[b] Units of cm^{-5} arcmin^{-2} for the thermal components, and photons keV^{-1} cm^{-2} s^{-1} arcmin^{-2} at 1 keV for the power-law components.

one centered on the filament, and two positioned to the W and to the E of it. These regions are shown in Figure 1. The regions were chosen to avoid the bright parts of the ICM, as well as emission from the SE galaxy group. The emission in the W and E regions was modeled with a single thermal component, while the emission in the filament region was modeled with two thermal components– one describing ICM contamination, whose parameters were linked to those of the thermal component used to describe the W and E regions, and one describing emission from the filament. The spectra from the three regions were fitted simultaneously. Table 1 lists the best-fitting parameters obtained for a gas metallicity of 0.2 solar. Varying the metallicity causes only minor changes to the best-fitting parameters, well within the statistical uncertainty ranges. In the JUPYTER notebook supporting this letter, we also show the results obtained for metallicities of 0 and 0.1 solar.

The XSPEC normalizations of the thermal components listed in Table 1 are defined as:

$$\mathcal{N} = \frac{n_e\, n_H\, V}{10^{14}\, \pi\, S_{reg}\, D_A^2\, (1+z)^2}\,,$$

if we assume the density to be constant in each region, where n_e is the electron number density, n_H is the hydrogen number density, V is the volume of the region, S_{reg} is the projected area of the region, D_A is the angular size distance to the cluster, and z is the cluster redshift.

To calculate the density of the filament in the region shown in Figure 1, we assumed this region has an elliptic

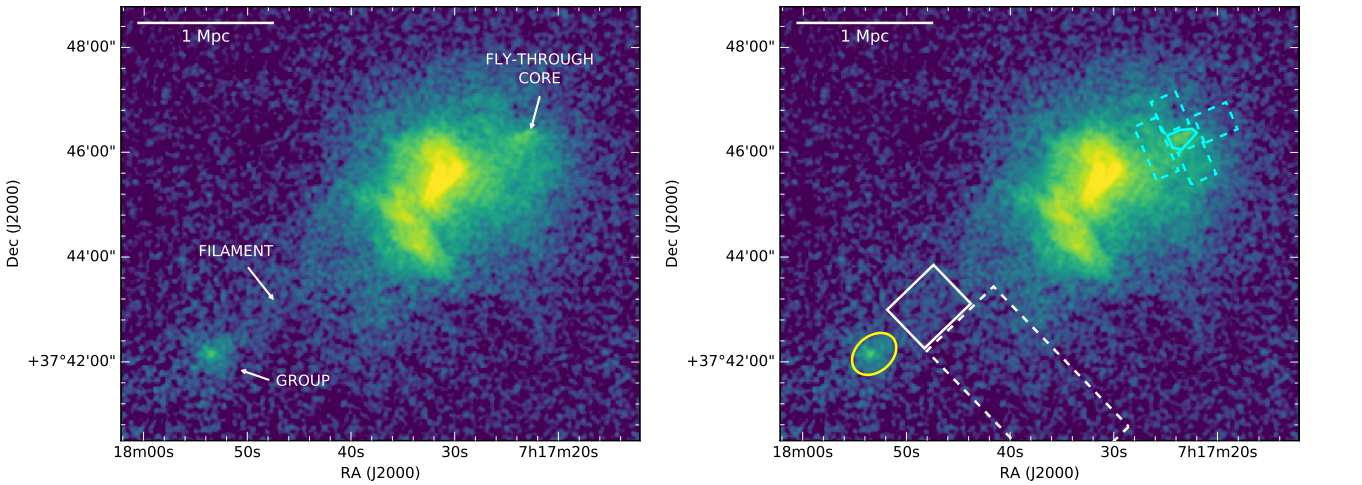

Figure 1. *Left:* Chandra $0.5-4$ keV surface brightness map of MACS J0717.5+3745, showing the features discussed in this work. The image was exposure- and vignetting-corrected. Point sources were subtracted and the gaps were filled by sampling the regions surrounding the point sources. The gaps were filled to create a more visually appealing figure. However, the imaging analysis was done on images that did not have the gaps filled. The images used in the analysis are available online as supporting material. *Right:* Regions used in the spectral analysis. The regions of main interest are drawn in solid lines, while the regions used to characterize the contaminating/surrounding emission are drawn in dashed lines. The best-fitting parameters obtained for the gas in these regions are listed in Table 1.

cylinder geometry. Jauzac et al. (2012) determined that the filament is inclined at 75 degrees with respect to the plane of the sky, and has a diameter of ~ 1.6 Mpc and a length of ~ 19 Mpc. Therefore, we assumed the region from which we extracted the spectrum of the filament to be an elliptic cylinder with a length:

$$L = \frac{l_{\rm box}}{\cos 75^\circ} \approx 1.8 \text{ Mpc}$$

where $l_{\rm box}$ is the length of the box region in Figure 1, and a base with major axis $a = 0.8$ Mpc and a minor axis equal to the length of the box in Figure 1, i.e. $b \approx 0.2$ Mpc. The volume of this region is $V = \pi a\, b\, L \approx 0.9$ Mpc^3. We further assumed that $n_{\rm e} = 1.2\, n_{\rm H}$ (Böhringer & Werner 2010). The area of the filament region shown in Figure 1 is 1.2 arcmin^2. Therefore, for an XSPEC normalization of $\sim 4\times10^{-5}$ cm^{-5} arcmin^{-2} (Table 1), the electron number density is $\sim 1.4\times10^{-4}$ cm^{-3}. Assuming the total density of baryons to be 4.4% of the critical density(Kirkman et al. 2003), the filament is overdense by a factor of ~ 300 compared to the mean baryon density of the Universe. Our result is roughly consistent with that of Jauzac et al. (2012), who used lensing data to calculate a filament over-density factor of 206 ± 46. Our result is also consistent with the upper range overdensities predicted from numerical simulations of cosmic filaments (e.g., Gheller et al. 2015).

For the density calculated above and assuming a baryon fraction of 0.15 (Mantz et al. 2014), the mass of the filament in the region from which the spectra were extracted is $\sim 2\times10^{13}$ M$_\odot$. Alternatively, we can parametrize the transversal gas density profile of the filament as the sum of two power-laws, following the results shown in fig. 17 of Gheller et al. (2015). Therefore, we approximated the transversal gas density profile as:

$$\rho_{\rm H}(r) = 1.7{\times}10^{-29}\left(\frac{r}{r_{\rm fil}}\right)^{-0.84} + 1.5{\times}10^{-29}\left(\frac{r}{r_{\rm fil}}\right)^{0.67}.$$

Using the equation above, the baryonic (total) mass of the filament in our spectral extraction region is just $\sim 7\times10^{11}$ M$_\odot$ (5×10^{12} M$_\odot$), thus confirming the fact that we are probing only the densest part of the filament. As the filament extends further out from the cluster, its density will decrease. This decrease in density is important when calculating the mass of the whole filament. For a filament length of 19 Mpc and a baryon fraction of 0.15, the transversal density profile above yields a total mass of $\sim (1-2)\times10^{14}$ M$_\odot$.

The calculations made above can be found in the supporting IPYTHON notebook accompanying this paper.

4. GROUP IN THE FILAMENT

The group of galaxies within the large-scale filament is located a little over 2 Mpc SE of the cluster center, chosen to be at RA = 07 : 17 : 30.025, Dec = +37 : 45 : 18.58 for consistency with Jauzac et al. (2012). The small size of the group and its large distance from the cluster implies that it is falling for the first time towards MACS J0717.5+3745, rather than having traversed the cluster from the NW to the SE.

We measured the temperature and the brightness of the group by extracting spectra from an elliptical region shown in Figure 1. We assumed a group metallicity of 0.2 solar. The best-fitting parameters are summarized in Table 1. The normalization is equivalent to a luminosity of $(1.05\pm0.09)\times10^{43}$ erg s^{-1} in the energy band $0.1-2.4$ keV. Based on the luminosity-mass scaling relations for galaxy groups (e.g., Connor et al. 2014), the group's luminosity corresponds to a mass of $\sim 5\times10^{13}$ M$_\odot$.

5. FLY-THROUGH CORE

Approximately 670 kpc NW of the cluster center, there is a bright X-ray core with a tail extending ~ 200 kpc towards SE, roughly in the direction of the large-scale filament discussed in Section 3. This morphology suggests that this core, seen 'flying' through the ICM of MACS J0717.5+3745 and ram-pressured stripped by the cluster's dense ICM, traveled NW along the SE filament and is seen after it traversed the brightest ICM regions. In essence, the core is a later stage of the group currently seen within the filament.

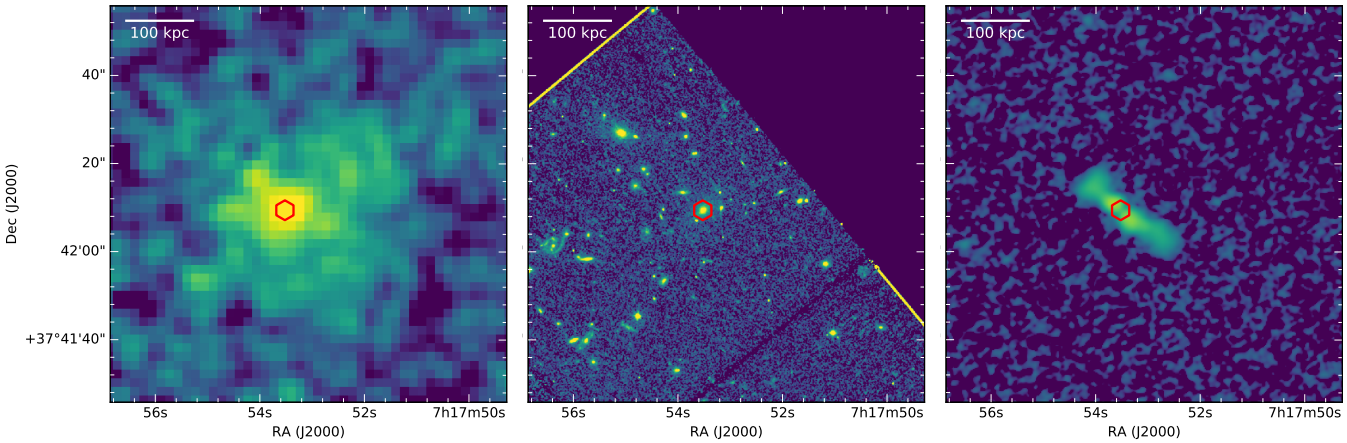

Figure 2. *Chandra* (left), *HST* (middle), and *VLA* (right) images of the region occupied by the galaxy group in the filament. The red hexagon marks the position of the group's BCG. The position of the BCG coincides with those of the radio AGN and of the X-ray peak.

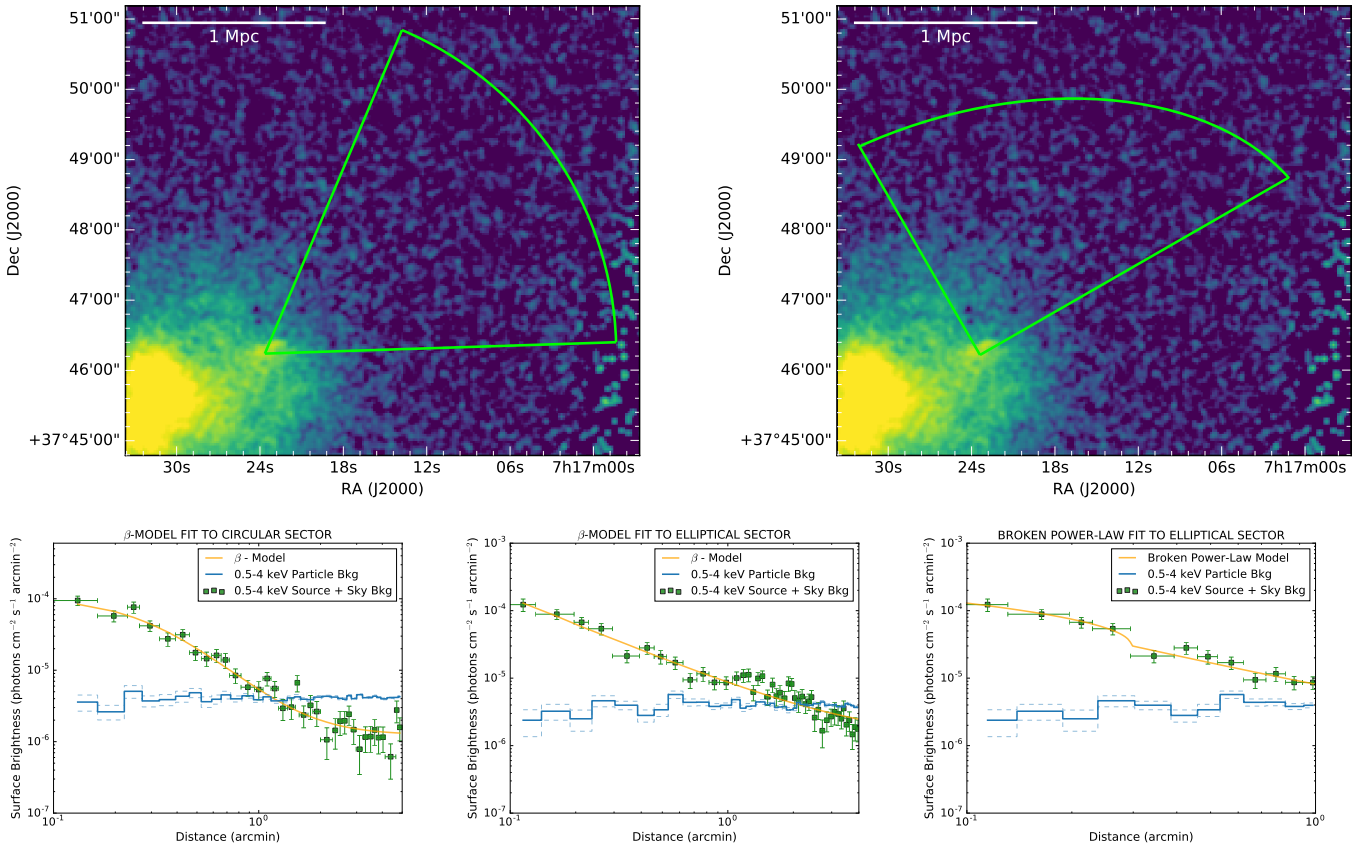

Figure 3. *Top:* Sectors used to model the surface brightness profile in front of the core. *Bottom:* Surface brightness profiles and best-fitting models. The instrumental background is shown in blue, with the uncertainty ranges on the background shown in dashed blue lines. For the elliptical sector, the surface brightness is plotted against the major axis of the ellipse. The best-fitting parameters of the broken power-law model are listed in Table 2.

The core is embedded (at least in projection) in the ICM of MACS J0717.5+3745. To determine the core's physical properties, we modeled the contamination from the ICM by extracting spectra N and S of the core. These spectra were modeled with a thermal component with a metallicity of 0.2 solar. We assumed the spectral properties were the same in the N and S regions. The spectra of the core were modeled as the sum of emission from the contaminating ICM and from the core itself. The spectra of the core and of the regions N and S of it were modeled in parallel. The best-fitting results are summarized in Table 1. The temperature of the core, $6.82^{+1.88}_{-1.36}$ keV, is consistent with the temperatures N and S of the core, in regions that are approximately at the same distance from the cluster center as the core. We also compared the core temperature with the temperatures ahead of (NW) and behind (SE) the core. The temperature decreases from $10.89^{+2.05}_{-1.27}$ keV behind the core, to $5.06^{+1.61}_{-0.98}$ keV ahead of the core. From these temperature measurements, we therefore find no evidence of a core colder than its sur-

Table 2
Best-fitting parameters of the broken power-law model fitted to the surface brightness of the core. Uncertainties are quoted at the 1σ level. The region from which the surface brightness profile was extracted, as well as the profile and best-fitting model, are shown in Figure 3.

α_1 [a]	α_2 [b]	Normalization photons cm^{-2} s^{-1} arcmin^{-2}	$r_{\rm break}$ arcmin	n_1/n_2 [c]	Sky background photons cm^{-2} s^{-1} arcmin^{-2}
0.62 ± 0.44	1.09 ± 0.15	$(1.82 \pm 1.11) \times 10^{-4}$	0.30 ± 0.05	1.61 ± 0.40	$(1.24 \pm 0.17) \times 10^{-6}$

[a] Power-law index at $r < r_{\rm break}$.
[b] Power-law index at $r > r_{\rm break}$.
[c] Density jump across the discontinuity.

roundings, nor of a temperature discontinuity (either a shock or a cold front) ahead of the core.

A cold front and a shock front would be expected ahead of the core, similarly to the features seen in the Bullet Cluster (Markevitch et al. 2002) and in front of the group NGC 4839 infalling into the Coma Cluster (Neumann et al. 2001) ***other citation needed here for the cold front***. We searched for possible evidence of a cold/shock front by modeling the surface brightness profile of the group. The sectors from which the surface brightness profiles were extracted are shown in the top panels of Figure 3. We chose two sectors: a circular sector with an opening aligned with the apparent direction of motion of the core, and an elliptical sector with an opening and ellipticity aligned with a possible edge observed by eye in the surface brightness map. The models fitted to these surface brightness profiles are shown in the bottom panels of Figure 3. The surface brightness profile extracted from the circular sector is well-fitted by a β-model. In this profile, there is a suggestion of an edge near ~ 0.3 arcmin, but a surface brightness model based on a broken power-law density model did not significantly improve the fit. In the surface brightness profile extracted from the elliptical sector, this possible edge becomes clearer. A β-model fit to this profile provides a good fit at high radii, but not at distances below $\lesssim 0.5$ arcmin. As seen in the bottom-right panel of Figure 3, a broken power-law density model follows the data closer. The best-fitting broken power-law density model fitted to the surface brightness profile in the elliptical sector has a density jump of 1.88 ± 0.35 at ≈ 0.27 arcmin from the center of the sector. The best-fitting parameters for the broken power-law model are summarized in Table 2.

The density discontinuity is at the very edge of the core. Therefore, we speculate that the discontinuity is associated with a cold front rather than with a shock front. The failure to find a temperature discontinuity associated with the density jump is likely due to a combination of poor count statistics and hot gas projected onto the core. The latter would also dampen the observed density jump, in which case our measurement of the jump amplitude is only a lower limit.

6. SUMMARY

MACS J0717.5+3745 ($z = 0.546$) is a massive galaxy cluster selected as one of the six Frontier Fields targets. The cluster is the most morphologically complex merger, being the site of collisions between at least four subclusters. SE of the cluster, there is a large-scale cosmic filament that was first reported by Ebeling et al. (2004). Some of the subclusters involved in the merger have likely traveled along this filament before colliding with the previously existing structure. Jauzac et al. (2012) determined from optical data that the filament is ~ 19 Mpc long and ~ 1.6 Mpc wide. Part of the filament that is near the cluster is also visible at X-ray wavelengths. So far, the thermodynamic properties of large-scale filaments have only been studied in a handful of merging clusters (Werner et al. 2008; Eckert et al. 2015; Bulbul et al. 2016). Here, we used deep *Chandra* observations of MACS J0717.5+3745 to study the properties of the large-scale filament extending SE of the cluster center, and those of the substructures along the filament. Below is a summary of our results:

- The filament has a temperature of $1.58^{+0.51}_{-0.25}$ keV and a density of $\sim 10^{-4}$ cm^{-3}. These are consistent at the 90% confidence level with the properties of the other filaments studied in X-ray (Werner et al. 2008; Eckert et al. 2015; Bulbul et al. 2016).
- The filament is over-dense by a factor of ~ 300 compared to the mean baryon density of the Universe.
- The total mass contained in the X-ray-bright region of the filament is $\sim 2 \times 10^{13}$ M$_\odot$. Approximating the transversal density profile of the filament with the model presented by Gheller et al. (2015), the mass of the whole filament (i.e. considering its full length of 19 Mpc) is $(1-2) \times 10^{14}$ M$_\odot$.
- A little over 2 Mpc SE of the cluster center, embedded within the filament, there is a galaxy group with a temperature of ~ 3 keV and an X-ray luminosity of $\sim 10^{43}$ erg s^{-1} in the energy band $0.1-2.4$ keV. The mass of the group is estimated to be $\sim 5 \times 10^{13}$ M$_\odot$. This group is likely approaching the cluster for the first time.

GAO acknowledges support by NASA through a Hubble Fellowship grant HST-HF2-51345.001-A awarded by the Space Telescope Science Institute, which is operated by the Association of Universities for Research in Astronomy, Incorporated, under NASA contract NAS5-26555. R.J.W. is supported by a Clay Fellowship awarded by the Harvard-Smithsonian Center for Astrophysics.

This research made use of APLPY, an open-source plotting package for PYTHON hosted at http://aplpy.github.com, and of ASTROPY, a community-developed core PYTHON package for Astronomy (Astropy Collaboration et al. 2013). This research has also made use of NASA's Astrophysics Data System, and of the cosmology calculator developed by N. Wright (Wright 2006).

The surface brightness modeling used PYXEL, a PYTHON open-source modeling package for X-ray astronomy.

The optical data shown in the paper is based on observations made with the NASA/ESA Hubble Space Telescope, and obtained from the Hubble Legacy Archive, which is a collaboration between the Space Telescope Science Institute (STScI/NASA), the Space Telescope European Coordinating Facility (ST-ECF/ESA) and the Canadian Astronomy Data Centre (CADC/NRC/CSA).

REFERENCES

Astropy Collaboration, Robitaille, T. P., Tollerud, E. J., et al. 2013, A&A, 558, A33
Böhringer, H., & Werner, N. 2010, A&A Rev., 18, 127
Bulbul, E., Randall, S. W., Bayliss, M., et al. 2016, ApJ, 818, 131
Connor, T., Donahue, M., Sun, M., et al. 2014, ApJ, 794, 48
Davé, R., Cen, R., Ostriker, J. P., et al. 2001, ApJ, 552, 473
Dietrich, J. P., Schneider, P., Clowe, D., Romano-Díaz, E., & Kerp, J. 2005, A&A, 440, 453
Ebeling, H., Barrett, E., & Donovan, D. 2004, ApJ, 609, L49
Ebeling, H., Barrett, E., Donovan, D., et al. 2007, ApJ, 661, L33
Ebeling, H., Edge, A. C., & Henry, J. P. 2001, ApJ, 553, 668
Eckert, D., Jauzac, M., Shan, H., et al. 2015, Nature, 528, 105
Einasto, M., Einasto, J., Tago, E., Dalton, G. B., & Andernach, H. 1994, MNRAS, 269, 301
Elvis, M., Plummer, D., Schachter, J., & Fabbiano, G. 1992, ApJS, 80, 257
Feldman, U. 1992, Phys. Scr, 46, 202
Gheller, C., Vazza, F., Favre, J., & Brüggen, M. 2015, MNRAS, 453, 1164
Jauzac, M., Jullo, E., Kneib, J.-P., et al. 2012, MNRAS, 426, 3369
Kalberla, P. M. W., Burton, W. B., Hartmann, D., et al. 2005, A&A, 440, 775
Kirkman, D., Tytler, D., Suzuki, N., O'Meara, J. M., & Lubin, D. 2003, ApJS, 149, 1
Ma, C.-J., Ebeling, H., & Barrett, E. 2009, ApJ, 693, L56
Mantz, A. B., Allen, S. W., Morris, R. G., et al. 2014, MNRAS, 440, 2077
Markevitch, M., Gonzalez, A. H., David, L., et al. 2002, ApJ, 567, L27
Mastropietro, C., & Burkert, A. 2008, MNRAS, 389, 967
Medezinski, E., Umetsu, K., Nonino, M., et al. 2013, ApJ, 777, 43
Neumann, D. M., Arnaud, M., Gastaud, R., et al. 2001, A&A, 365, L74
Springel, V., & Farrar, G. R. 2007, MNRAS, 380, 911
Springel, V., Frenk, C. S., & White, S. D. M. 2006, Nature, 440, 1137
Werner, N., Finoguenov, A., Kaastra, J. S., et al. 2008, A&A, 482, L29
Willingale, R., Starling, R. L. C., Beardmore, A. P., Tanvir, N. R., & O'Brien, P. T. 2013, MNRAS, 431, 394
Wright, E. L. 2006, PASP, 118, 1711
Zitrin, A., Broadhurst, T., Rephaeli, Y., & Sadeh, S. 2009, ApJ, 707, L102